1-1-1980

Development of a helium-neon laser based flow cytometer for evaluation of particulate matter

Sham Persaud
Iowa State University

Development of a helium-neon laser based flow cytometer for evaluation of particulate matter

by

Sham Persaud

A Thesis submitted to the
Graduate Faculty in Partial Fulfillment of the
Requirements for the Degree of
MASTER OF SCIENCE

Major: Biomedical Engineering

Iowa State University
Ames, Iowa

1980

TABLE OF CONTENTS

INTRODUCTION

Flow cytometry, using laser illumination, is becoming an increasingly popular tool in cell research and clinical medicine for measuring parameters such as cellular DNA content, RNA content, cell and nuclear size, light scatter, and fluorescence anisotropy. These parameters are usually displayed as either one or two dimensional histograms. In many pathological conditions, neoplastic cells may be recognized by optically measurable changes in constituent substance and not the presence or absence of a particular substance. For instance, malignant cells show an increase in nuclear fluorescence due to the increase in DNA material. From an experimental viewpoint, flow systems utilizing light scatter technique, are particularly attractive, since neither staining nor fixation is required, thus requiring a minimal amount of preparation time. From a clinical standpoint, flow systems offer the advantages of high speed analysis, unique statistical precision and sensitivity, routine measurements not previously possible on large number of cells within a population, the reduction of slide-related artifacts, and the capability of studying viable cells which can be reused.

Laser flow microphotometry describes systems where particles (often mammalian cells) in suspension are made to flow through a special chamber one at a time (like beads on a string) for exposure to a focused laser beam. As each cell crosses the laser beam, it produces an optical scatter pulse of duration equal to the cell transit time across the beam. These pulses are detected, amplified and analyzed. In most instances, the analysis is done by pulse-height analyzers or by minicomputers, depending upon

how many parameters are measured. Much information about the size and internal structure of unstained and unfixed biological cells and other microscopic particles can be obtained from the light-scattering properties alone (1,2).

In most flow systems, some type of sheath flow configuration is used to align the cells for exposure to the exciting light. Sheath-flow is generally established within a suitable flow-cell with the carrier or sheath fluid representing the bulk of the flow. The cell suspension is injected along the axis of a converging and accelerating sheath of cell-free fluid at a point where the fluid velocity is low. Just prior to entering the illuminating and viewing area, the entire flow moves through a constriction orifice which narrows the total flow and core (cell stream) such that the cell stream is small (usually about 20 micrometers) as it intersects the laser beam.

This thesis describes the development of an economical sheath-flow chamber made almost entirely out of Plexiglas (Rohm and Haas, Philadelphia, PA). The chamber design was based on the principle first employed by Crosland-Taylor (3). The sensitivity of this instrument was established for latex spheres ranging from a uniform population (3.49 micrometers) to a mixed population (3.49 to 14 micrometers). To demonstrate the capability of light scattering to distinguish biological cells of different size and morphology, white blood cells (leukocytes) which represent a multiclass population, were chosen as test cases. An attempt was made to qualitatively classify unstained white blood cells based solely on their light-scattering characteristics, and the results were compared with

those obtained by trained human observers using conventional wedge smears stained with Wright's stain.

LITERATURE REVIEW

Over the years, many attempts have been made at automating cytological examination of human exfoliative material, all geared towards clinical diagnosis. Through the use of automation, normal samples can be screened and the ever-increasing workload of the cytotechnologists and pathologists who are primarily responsible for these diagnostic evaluations can be reduced, thus leaving them with more time to spend on the proper evaluation of the abnormal samples which may dictate treatment or surveillance of the patients by their clinicians.

Image analysis and flow system analysis are the two main approaches to automation in cytology. In the first instance, cells are affixed to microscope slides, stained, and examined optically by trained human observers or by pattern recognition computers which have the capability of providing large amounts of information on each individual cell in a population. The power of this method lies in the ability of the computer software to extract sufficient information to make important and unique distinctions between cells. In flow systems analysis, the emphasis is on speed. This consequently decreases the resolution compared with the slower, high resolution image analysis. In flow systems, cells in a constrained stream are made to flow at relatively high speeds past one or more detectors arranged strategically at different angles with respect to the incident illumination beam. In the case of fluorescent studies where the specimen is labelled with a fluorescent stain specific for the cell or organelle of interest, the detectors are often placed at 90° with respect to the exciting beam and the cell stream to maximize the detection without interference

from the main beam-trap, and to minimize blocking requirements of barrier filters. The fluorescent light emission occurs at a longer wavelength than the incident light, whereas in light scatter studies, the incident light experiences no appreciable change in wavelength, thus the detectors are placed at various angles depending upon the parameter being measured.

The scattering of light by cells in flow systems has been used to determine their size (1,4), to differentiate viable from nonviable cells (5) and to distinguish between cell types (6). The total light scattered by a cell and the angular distribution of this light are related not only to the cell and nuclear diameters but also to smaller organelles, and to the refractive indices of the various cellular constituents (7). Cells with axial symmetry about the direction of flow will yield the same signal upon rotation around that axis; however, asymmetrical cells, such as epithelial and red blood cells, may produce a scatter signal that is dependent upon their orientation (8,9).

Whenever light impinges upon a cell, it may not be completely absorbed but partially deflected (scattered) by the processes of reflection, refraction and diffraction with the observed light dependent upon the size and refractive index distribution of the cell, the refractive index of the medium, the wavelength of the incident light and the angle of observation.

Reflection is the process whereby light is reflected back into the surrounding medium from a particle's surface when it is illuminated. When the surface is smooth, the angle of incidence equals the angle of reflection, while rough surfaces diffuse light in many directions. If the roughness of the particle's surface is small compared to the particle size and the wavelength of the incident light, the roughness will have very little

effect on scattering.

Refraction is the phase shifting and bending of the rays due to the different relative index of refraction for the nucleus, cytoplasm and the surrounding medium.

The presence of a particle in the beam of light perturbs the electromagnetic field of the light wave. This disturbance at the edge of the particle is called diffraction. This spreads light to some extent into the region that is not directly exposed to the oncoming wave. The general features of diffraction are described by Huygens' principle (10).

The angle of measured light-scatter is determined by the position of the detectors. In the multiangle light scattering system shown in Figure 1 (11), light scattered from single cells can be collected simultaneously at up to 32 angles in the forward direction between 0° and 21°, and in the backward direction between 175° and 177°.

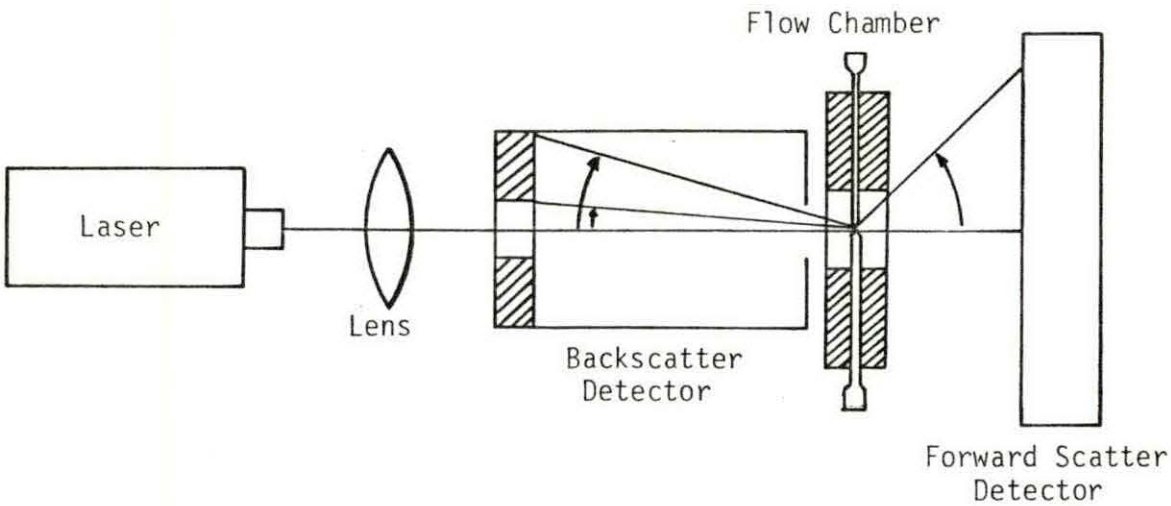

Figure 1. Multiangle light-scattering system. Scattering angles are defined by position of the detectors.

Light scattered in the forward direction is dominated by diffraction processes; thus, the intensity of light scattered at small angles (0.5-2°) dominates the observed intensity distribution, and is indicative of the size of the scattering particle (1). Scattering at intermediate angles (5-80°) is principally due to refraction and to a lesser extent diffraction and yields information about internal architecture, while very large angle scattering (90-180°) is mostly reflection from the surface or from internal surfaces where the index of refraction changes. For a thorough treatise on the complex phenomenon of light scattering, the interested reader is referred to the text by Kerker (12) and review articles by Wyatt (13) and Brunsting and Mullaney (2).

Flow cytometry has been under development since the middle 1950s from an effort initially intended to count and later to size particles. Many of these prototype systems evolved into sophisticated analytical tools for rapidly quantitating multiple chemical and physical properties of the individual cells or cellular constituents of inhomogeneous populations. During most of this time, efforts were directed primarily toward the development of new and improved instrumentation. A brief historical review of the significant developments in automated cytometry follows.

An early attempt to count cells in suspension started in the 1930s and 1940s (14). This method, known as "turbidimetry" used a photoelectric device to measure light transmission through a suspension of cells. The major limitation was that the measurements were influenced by anisocytosis (variation in cell size).

A bright field photometric method to count cells automatically while in flow was reported by Moldavan (15) in 1934. Red blood cells in suspen-

sion were forced through a fine capillary tube located on a microscope stage and each passing cell was counted by a photoelectric apparatus attached to the ocular. The experiment was unsuccessful due to difficulties encountered in focusing of cells in the capillary tube, cell clumping, and lack of sensitivity in the phototube system.

A few years later, Gucker et al. (16) developed a photoelectronic counter utilizing flashes of light scattered by colloidal particles traversing a small space under dark-field illumination. The apparatus consisted of (a) a chamber in which a stream of very dilute smoke passed through an intense light beam, scattering flashes of light forward onto a photomultiplier tube, (b) a pulse amplifier and (c) a trigger circuit which actuated a mechanical counter. The device was successfully tested with uniform particles (dioctyl phthalate) of diameter down to 0.6 micrometer and with aerosols of ellipsoidal spores (Bacillus sp.) averaging about 0.8 x 1.2 micrometers.

A year later, Lagercrantz (17) constructed a photoelectric apparatus for counting individual microscopic cells in fluid suspension by using the capillary tube method (15) and dark-field illumination. It was unsuccessful due to light reflection from the capillary tube into the microscope objective lens, causing loss of dark background and thus creating a low signal-to-noise ratio in the optophotoelectric measurement system. It was also difficult to force cells through the capillary tube which had the same size as the cells to be counted. By increasing the capillary tube size, the problem encountered was focusing of the cells (as seen in the work of Moldavan in 1934). Even though the experiment was unsuccessful, Lagercrantz observed that when a slide or counting chamber, charged with a

dilute suspension of cell, was moved with respect to the objective, distinct light signals were obtained. This observation was the initiation of the scanning method from which numerous automatic scanning techniques have evolved.

In 1953, Crosland-Taylor (3) applied the laminar sheath flow principle first described by Reynolds (18) in 1883 to design a chamber for optical counting of red blood cells. An aqueous suspension of cells was slowly injected into a faster stream of fluid flowing in the same direction; the latter provided a laminar sheath surrounding and aligning the particles. This system permitted the single-file alignment of cells in a rapidly flowing fluid, and it did not use a "minute" orfice which tended to clog very easily. It was not until a decade later that the potential of this device was recognized and utilized. Almost all flow cytometry instruments today make use of the sheath-flow principle described by Crosland-Taylor.

In 1955, Frommer (19) reported a direct reading blood-count meter made from a microscope slide and a cover glass. This chamber design was used a few years later by Steinkamp (20) for counting and sizing of biological cells through the use of fluorescence and dark-field (light scatter) optical properties. Cells in suspension were made to flow through a dark-field illuminated inspection zone that was monitored by a photomultiplier tube. The cell concentration was determined on the basis of the time relationships between the presence and absence of cells in the inspection zone. This device yielded results independent of particle size, rate of sampling and quantity sampled. There was also good agreement between instrument count and manual hemocytometer count of both erythrocytes and leukocytes of normal and leukemic patients.

An electrical technique for high speed cell counting and sizing of microscopic particles was reported by Coulter (21) in 1956. This became the basis for the first viable flow analyzer. Individual particles suspended in an electrolyte, typically saline, were made to flow through a constricted orifice by a suction pump. Depending on the particle size, the orifice diameter ranged from 30 to 300 micrometers. An adjustable constant current source was connected on either side of the orifice. Each particle passing through the orifice momentarily impeded the flow of current, thereby creating a voltage change between the electrodes. After suitable amplification, these voltage pulses were amplified and tallied electronically as cell counts. Since its invention, the Coulter automatic cell counter has been used extensively by different groups of researchers for volume determinations of cells ranging from bacteria (22) to various cell types (23, 24,25). These researchers concluded that the amplitude of the voltage pulses generated by the passage of a particle through the Coulter aperture was linearly related to the particle volume as proposed earlier by Kubitschek (22). About a decade later, Kachel (26) found that the height and shape of the voltage pulses were dependent on the applied constant current, the geometrical dimensions of the orifice, electrical conductivity of the suspending medium and the particles, the shape of the particles and lastly, the trajectory of the particles in the orifice. Identical spheres having different trajectories gave voltage pulses of different shapes and durations (27) as shown in Figure 2. Axially focused particles (trajectory a of Figure 2 A) were subjected to the highest accelerations, had the shortest transit times and gave the most symmetrical pulses (pulse a of

Figure 2 B). Relative to these pulse forms, those particles with more peripheral trajectories (the edge trajectory e) were distorted and resulted in overestimation of relative particle volume (pulses c to e). Similar results were obtained by an optical time-of-flight cell sizing method (28). This is probably due to the Gaussian nature of the intensity across the incident laser beam.

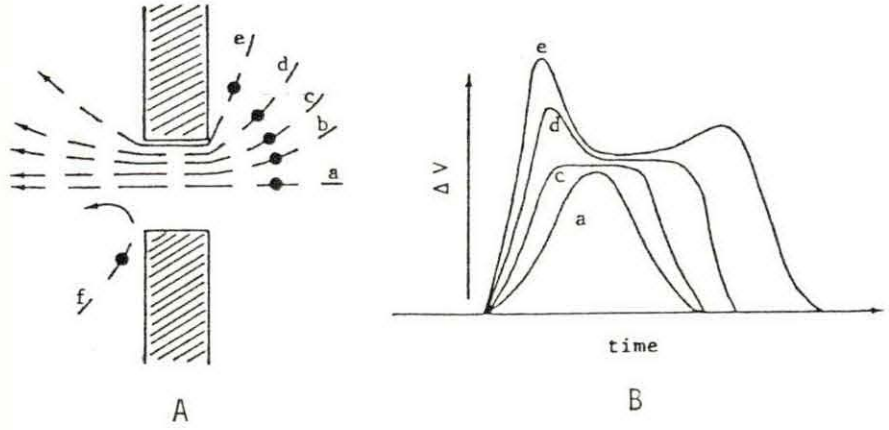

Figure 2. Standard Coulter orifice with A)orifice particle trajectories and B)corresponding pulse forms [from Von Behrens and Edmondson (27)].

In 1965, Kamentsky et al. (29) reported a two-parameter, microscope-based flow cytometer that measured absorption and back-scatter illumination of unstained cells at rates exceeding 500 cells per second. Photometric measurement of human cells from different parts of the body were made at 253.7 nm (U.V. absorption) and 410.0 nm (light scatter). Cells were individually measured while flowing at a rate of 0.5 ml per minute through a 100 micrometer wide x 100 micrometer deep bow-tie shaped channel cut into a quartz microscope slide which served as the flow chamber. The chamber (slide) was mounted on the stage of a microscope with a mercury

arc light source focused on the flow chamber by a condenser. Two photomultiplier tubes were arranged to measure light absorption and light scatter from the stream. The oscilloscope display pattern of neoplastic cells showed considerable variation from normal cells. Cancer-cell suspensions from tumors consistently showed cells with higher absorption at 253.7 nm when plotted against the light scatter signal.

Flow cytometers were improved by Van Dilla et al. (30) in 1969 by incorporating a laminar sheath-flow chamber and an argon-ion laser. The sheath-flow technique first utilized by Crosland-Taylor (3) was used to confine cells to the center of the flow stream. Fluorochrome stained cells flowed at a rate of 10^4 to 10^5 cells/minute in a narrow stream (diameter 50 micrometers) across a beam of exciting light (diameter 100 micrometers); the resultant fluorescent light pulses were measured perpendicularly to both cell stream and light beam by a photomultiplier. The electrical pulses were amplified and analyzed for amplitude by a multichannel pulse-height analyzer and were found to be proportional to the fluorescence intensity. Unlike earlier systems, no microscope and a minimum of optics were used. A simple lens of 20 cm focal length focused the laser beam to the desired 100 micrometer diameter at the cell stream, and a pair of f/1.6 movie projection lenses transferred the signal to a low noise photomultiplier tube. A helium-neon laser and the same flow chamber were used by Mullaney et al. (31) to study small-angle forward scattering of cells in flow at rates of 10^4 to 10^5 cells/minute. Scattered light between 0.5° and 2° was collected from individual particles, 5 micrometer to 20 micrometer diameter, ranging from plastic monospheres to mammalian cells. The results were found to be in good agreement with results obtained using

a Coulter Counter (Coulter Electronics, Inc., Hialeah, FL) and by direct measurements of cell size by light microscopy. However, in cases where it was necessary to fix cells, light scatter results were more reliable than Coulter distributions due to the fixative which altered the electrical properties of the cell without producing a significant cell size change. They also found that small angle light scattering from several opaque samples showed no difference in observed scatter signal from transparent spheres of the same diameter, confirming that diffraction was the main scattering mechanism.

Fluorescent techniques, which paralleled the development of light scatter, had their beginning in the early 1950s with the development of a scanning apparatus for the differential detection of cancer cells prepared on microscope slide (32). The potential of this technique was not realized until approximately two decades later. In many biological applications to date, the emphasis is on fluorescent technique coupled with light scattering signatures to identify different cell types. For example, acridine dyes, especially acridine orange, have been widely accepted as fluorescent stains for nucleic acids in fixed plant and animal cells. Since this research study involves light scatter rather than fluorescence, the author will not delve into the theory of fluorochrome stains nor the detailed development of fluorometers. However, the avid reader is referred to the multiauthored text, FLOW CYTOMETRY AND SORTING (33) for more specific information on the cytochemistry of fluorochromes and its myriad of applications in cell biology, immunology, hematology and oncology.

In 1973, Holm and Cram (34) reported an improved flow microfluorometer for rapid measurement of cell fluorescence. The instrument was an improve-

ment of the system described by Van Dilla et al. (30). The chamber design was basically the same but the light focusing and collecting optics were different from those used by Van Dilla et al. (30). Instead of a simple 20 cm focal length lens, the laser beam was focused to an elliptical cross section at the cell stream by two cylindrical lenses of focal length 2 and 20 cm. The collecting optics consisted of a f/1.6 projection lens, a glass filter to block scattered light, followed by a similar second projection lens to focus the fluorescent light on a 200 micrometer pinhole. After passing through the pinhole, the light was made parallel by a small collimating lens and a prism was used to reflect the light on the photocathode of the photomultiplier. Single-cell suspensions were stained with a fluorescent dye specific to the cellular component of interest. Instrumental quality was demonstrated by measuring the fluorescence distribution of uniform 12 micrometer fluorescent plastic microspheres and was found to be capable of resolving two populations of microspheres differing in fluorescent intensity by 10%.

Later that year, Mullaney and West (35) reported a dual-parameter flow microfluorometer to simultaneously measure the light scattering and fluorescence of stained mammalian cells. The flow chamber was of the same design reported previously by Mullaney et al. (31). Fluorescent light was detected at 90° to the incident beam by a photomultiplier tube, and light scattered in the forward direction was focused onto a phototube. The instrument offered the possibility of improved signal-to-noise ratio on weakly fluorescent samples such as those occurring in immunofluorescent studies. The ability to obtain light scattering as well as fluorescent information on each cell in a population greatly extends the potential for

cell identification.

Identification of discrete classes of normal human peripheral lymphocytes by multiparameter flow analysis was reported by Steinkamp and Romero (36). Human leukocytes stained with acridine orange were separated into four groups consisting of granulocytes, monocytes and two types of lymphocytes. Identification was on the basis of green/red fluorescence ratio measurement which characterized nucleus and cytoplasmic staining properties.

A new high speed instrument for multiparameter analysis and separation of cells and subcellular particles under computer control was reported by Arndt-Jovin and Jovin (37). Like previous instruments, the new instrument incorporated a laser source for excitation of fluorescence and scattered light, a coaxial flow of particles and sheath fluid and the process of drop generation. However, the electronics enabled the multiparameter usage of up to 10 simultaneous signals. Five independent analog channels with a corresponding number of totally interchangeable sensors (detectors) were available for observation of particle fluorescence, light scattering, light absorption and excitation intensity. Finally, the instrument incorporated on-line computer control of data acquisition and analysis, data storage and display, and drop charging for five sorting categories.

Mansberg et al. (38) reported the commercially available Hemalog D (Technicon Instruments Corp., Tarrytown, NY) system which performed automatic differential white cell counts utilizing the principles of cytochemistry, electro-optical measurements and signal processing. Using anticoagulated whole blood and an automated continuous flow staining technique, the system could process one sample per minute, that is, 30,000 cells per

sample compared to conventional manual methods of 100 leukocytes per sample by trained technicians. The decision logic classified individual cells based on size and intensity of staining as they flowed past detectors designed to measure light loss and light scattering simultaneously. The flow cell was fabricated of stainless steel components and optically flat glass windows. Sheath flow was used to constrain the stream from the effluent manifold from 250 micrometers to 60 micrometers. The system incorporated three flow chambers with separate optical configurations. However, there was a single tungsten halogen lamp acting as a common light source for the three optical systems. This system has the advantage of processing large number of cells in a short time span. The precision makes acquisition of sequential data on a single patient (as in cancer patients undergoing chemotherapy) more meaningful and diagnostically valuable.

In 1975, Salzman et al. (39) found that unstained leukocytes can be classified into distinct morphologic types based on a measurement of light scattered by each cell at two different angles. A phototube was positioned one degree from the laser beam to measure the intensity of light scattered by a cell in the forward direction, and a photomultiplier tube was used to collect light scattered from a cell at 90°. The data were analyzed by a two-parameter pulse-height analyzer. Three distinct cell types consisting of lymphocytes, monocytes and neutrophils were identified.

A multiangle light-scattering flow system for cell characterization was reported by Salzman et al. (11). Prepared cervical and vaginal specimens were made to flow at high speed (60,000 cells/minute) through a focused helium-neon laser beam and the scatter pattern from each cell was sampled simultaneously at up to 32 angles between 0° and 30° with respect

to the laser beam axis. Because the detection rings span 180° in azimuthal angle, the rings were not sensitive to cell rotation about the detector axis. The scatter pattern for each cell was transferred to a computer. The data indicated that a gynecological specimen diagnosed as invasive carcinoma could be distinguished from a normal gynecological specimen based only on the angular distribution of light scattered by individual cells.

In 1975, Eisert et al. (40) developed a simple particle analyzer using a modified, high speed, flow-through technique and absorption measurements of a continuous helium-neon laser beam. Size distributions of stained and unstained cells were derived from the pulse-shape analysis and the integration of absorption pulses. Cells ranging from 5 to 300 micrometers could be analyzed without altering or changing the flow chamber.

A flow cytometer for high efficiency light collection was reported by Skogen-Hagenson et al. (41). The chamber, an ellipsoid of revolution, was machined in two halves from solid brass and nickel-plated with a flash of gold for increased reflectivity. With this type of design they were able to collect about 60% of the total cell fluorescence for analysis compared to about 2.5% for conventional flow systems. Orientation and shape of particles about the flow axis were not as crucial as in earlier flow systems.

Lindmo and Steen (42) developed a relatively inexpensive, microscope-based, easy-to-operate flow cytometer with high resolution and stability. A fluorescence microscope was chosen because it provided high aperture optics for both excitation and fluorescent light. A laminar flow was created on a microscope cover slip by means of a jet of water directed onto the glass at an angle. Cells were centered in the jet by hydrodynamic

focusing. A photomultiplier tube was mounted on the eyepiece of the binocular of the microscope. Sample flow rates on the order of 10^3 cells/second could be analyzed. Pulses from the photomultiplier tube were fed to a multichannel analyzer which consistently yielded DNA histograms with a coefficient of variation below 1.0%.

A new flow cytometer for detection and discrimination of individual viruses based on differences in their light scattering was reported by Hercher et al. (43). The chamber was of an orthogonal configuration with the sample flowing downward along the vertical axis and with illumination and collection optics along the horizontal axis. The light employed was a 1 watt continuous wave argon-ion laser which was focused such that the beam was 10 times greater in diameter than the cell stream in order to expose particles regardless of their position within the stream. A tapered quartz capillary tube served as the chamber and the sample stream, which was driven by a microliter syringe pump, was confined to a small stream by deionized water which served as the sheath fluid. The sample stream diameter could be varied between 2 and 20 micrometers. The capillary was enclosed by a water-filled chamber having a single drain outlet directly below the capillary tip. Both fluorescent and scattered light signals could simultaneously be detected through the use of a dichroic beamsplitter and two photomultiplier tubes. However, only light scatter was used to detect suspensions of viruses, viral capsids and latex spheres. Mixtures of latex spheres in the size range 0.091 to 0.765 micrometer were well-resolved. Although some types of viruses produced very sharply defined scatter signals, other types could not be separated on the basis of scattered light histograms alone. However, by augumenting the scatter signal

by a fluorescent signal, better discrimination could be made between similar viruses.

SYSTEM DESCRIPTION

Overview

The most crucial part of the system is the flow chamber which is used to confine cells in the central part of the flow stream for exposure to the laser beam which is focused to a point source on the cell stream by means of a spatial filter and a spherical lens. Cells traversing the focused beam cause the light to be scattered in all directions. Light scattered in the forward direction is captured by a photomultiplier tube which has its photocathode in close proximity to the chamber. The pulses are amplified and fed into an oscilloscope for observing and photographing. A diagram of the entire system appears in Figure 3.

Flow Chamber

Flow chambers are classified as either "closed" or "jet-in-air" flow systems. The earlier flow chambers described by Van Dilla et al. (30), Mullaney et al. (31) and Holm and Cram (34) were "closed" systems wherein the measurement region is completely surrounded by a liquid medium. Simpler jet-in-air flow systems have become popular as a result of work by Bonner et al. (44) using a single laser beam to intercept the stream in air. Since their introduction, jet-in-air systems have been used extensively to rapidly identify and separate functionally distinct groups of viable cells based on their light scattering characteristics or fluorescence intensities or a combination of both.

A closed type chamber design was selected for this research due to

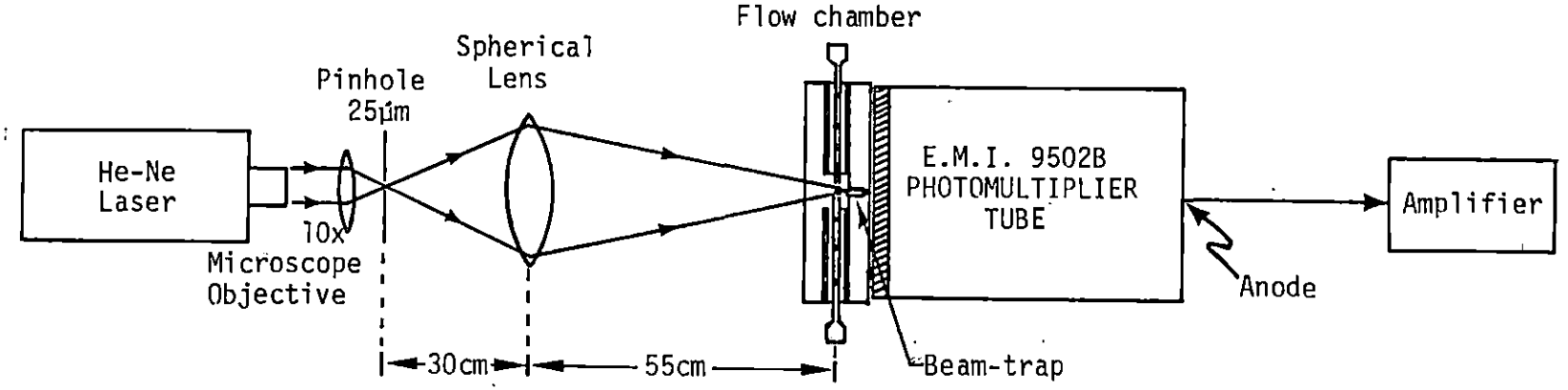

Figure 3. Schematic diagram of the flow system. The helium-neon (He-Ne) laser is focused by an achromatic lens to a point source which was slightly defocused in the flow chamber. Light scatter is collected by the photomultiplier tube and the anode signals are capacitatively coupled to the amplifier.

its suggested superior sensitivity and resolution over a cell stream jetted in air (45). The chamber design was a variation of the coaxial flow system originally developed by Crosland-Taylor (3) for counting red blood cells. By hydrodynamic focusing, cells are confined to the flow stream without mixing with the surrounding sheath of distilled water or saline solution. This helps to keep particlulate material away from the walls, minimizes clogging of the aperture, and forces the cells to move in almost identical trajectories at uniform speeds through the focal spot of the intense beam. In this way, each cell can receive uniform illumination during its transit time across the beam.

The chamber is fabricated almost entirely of Plexiglas with stainless steel hypodermic needles used for stream ports. It consists of three sections, namely front, middle and back plates, all of which are made from 3/8 inch (approximately 9.0 mm) thick Plexiglas. The front plate (5.2 x 5.2 cm) has a window (5 x 10 mm) in the center to permit the laser beam to intercept the cell stream. The inner side of this plate was machined to accommodate a glass microscope slide over the window to prevent attenuation and diffusion of the beam, and of course, loss of fluid from the chamber.

The center plate (5.2 x 5.2 cm) diagrammed in Figure 4 represents the main component of the chamber; it houses the sample-sheath coaxial assembly, debubbler, exit and cleaning ports. The center of this plate was drilled out to a 11/16 inch (approximately 1.7 cm) diameter.

The coaxial assembly is made out of two 1 1/2 inch (approximately 3.8 cm), 18 ga. and one 1 inch (approximately 2.5 cm) 27 ga. hypodermic needles with the bevel ground to a square end. The input 18 ga. needle

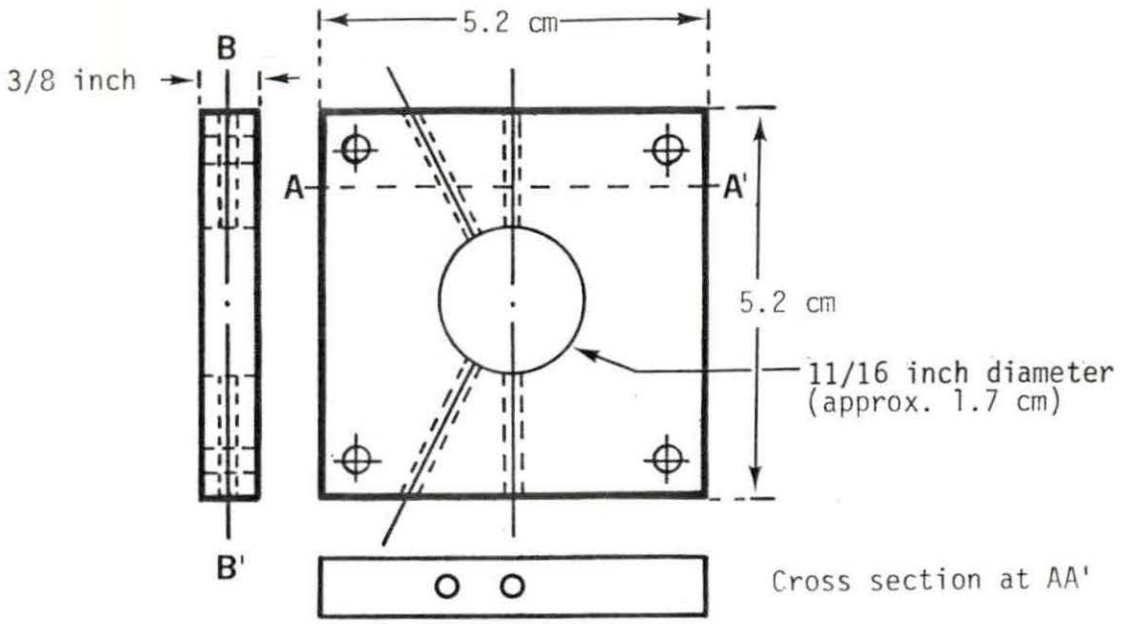

Figure 4A. Dimensional drawing of center plate.

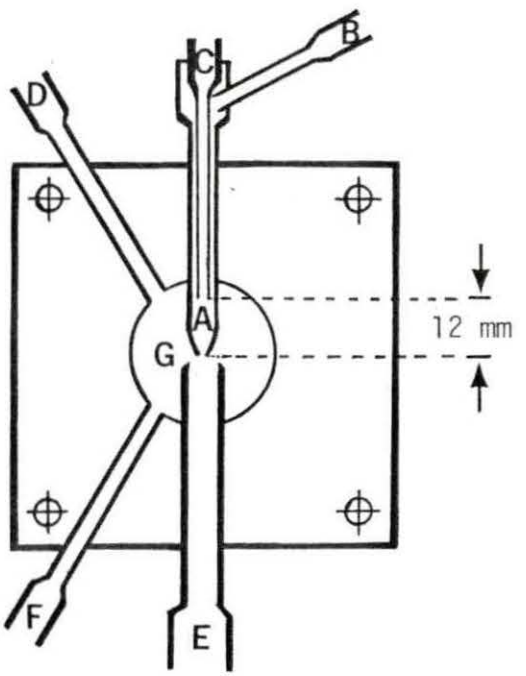

Figure 4B. Cross section of center plate of the flow chamber at BB'. A - central bore of chamber; B - sheath entry port; C - sample inlet port; D - debubbler; E - exit port; F - cleaning port; G - transition region.

(A in Figure 4) is swaged at the tip to reduce the internal diameter (0.8 mm). In this case, the internal diameter after swaging measures approximately 200 micrometers with the tip tapered for approximately 4 mm from the end of the needle. The other 18 ga. needle (sheath-entry port, B in figure 4) was epoxied to the plastic holder of the swaged needle at an angle of approximately 45°. Finally, the 27 ga. needle (sample-inlet port, C in Figure 4) is inserted into A until both needle holders were in close contact, and were epoxied. The distance between the tip of A and the tip of C is 12 mm as shown in Figure 4. On the same side of and adjacent to the coaxial assembly is the debubbler (D in Figure 4) positioned at approximately 45° to the tip of the coaxial assembly. The debubbler is used to remove air bubbles from the chamber by applying slight negative pressure with a small tuberculin syringe. The exit port (E in Figure 4) is carefully aligned on the side of the chamber, opposite the coaxial assembly such that the 2 mm space between the input and exit ports is in the center of the chamber. To facilitate cleaning and draining of the chamber, another drain (E in Figure 4) positioned at approximately 45° to the main exit port is installed such that the tip is at the periphery of the chamber. All of the ports are held in position with 5-minute Devcon (Devcon Corp., Danvers, MA) epoxy.

The back plate (10.4 x 5.2 cm) serves as the viewing window for the photomultiplier tube and the mounting bracket for the chamber. In addition, it houses the beam-trap which is made from 1/8 inch (outside diameter) copper tubing.

Since the size and position of the beam-trap dictates the minimum

scattering angle detectable, which in this case is approximately 23°, it is made as small as possible. Flaring the tubing obviously increases tube size which consequently, was found to decrease the collection angle and the amplitude of the detected signals. Instead of flaring, the inside of the 1/8 inch copper tubing was filed with a tapered file as shown in Figure 5. The entrance of the beam-trap after filing measured 3 mm. The narrow end of the 8 mm long tubing was crimped and soldered, and the inside was sprayed with flat black paint to reduce reflections from the beam. A partial hole to accommodate the beam-trap was drilled in the center of the inside back plate in the center of the space between the sample entry and exit ports of the center plate. The beam-trap was then carefully tapped into the snug fitting clearance hole until it was level with the inside surface.

To prevent leaks, gaskets made from Silastic (Dow-Corning Corporation, Midland, MI) sheeting are used between the plates. The chamber is held together by 4 pan-head 6-32 1 1/4 inch machine screws with the heads

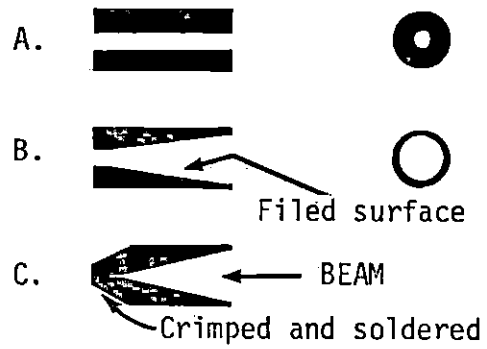

Figure 5. Beam-trap. A. copper tubing with its cross-section. B. copper tubing after filling. C. crimped and soldered beam-trap.

countersunk on the outside back plate to facilitate mounting of the photomultiplier tube in close proximity to the chamber as depicted in Figure 3.

Both the chamber and the photomultiplier tube with its associated voltage divider network are mounted on an aluminum block which in turn is mounted on a micromanipulator stage to allow precision alignment of the sample stream and laser beam. The photomultiplier tube is enclosed in a light-tight box made from Plexiglas and sprayed with flat black paint. Light can enter only by way of the flow chamber. To prevent accidental electrical shock, the dynode chain at the base of the tube is enclosed in an aluminum box which has BNC connectors for the high voltage supply and the anode signal.

To avoid movement of the chamber once positioned, a manifold with three 2-way valves is placed directly above the flow chamber. The valves are connected to the inlet ports of the sample, sheath and debubbler by flexible tubing.

Referring again to Figure 4, filtered distilled water or saline enters the central bore of the chamber (A) by the sheath entry port (B) and laminar ("smooth") flow is established in the 0.8 mm diameter cylindrical bore section of the sample-sheath needle. The flow then enters the tapered portion of the swaged needle which has an exit diameter of approximately 200 micrometers. The sample inlet port (C) on the axis of the main flow serves to introduce the particle suspension into the faster flowing sheath fluid. Cell-free sheath fluid flows around the sample inlet tube, accelerating and narrowing the core diameter. The fluids emerge coaxially from the 200 micrometer exit diameter with a cell stream

diameter of approximately 20 micrometers across a smooth transition region (G) where it is intersected by the focused beam. The combined flow leaves the chamber through the exit port (E). To prevent droplet formation at the outlet of the exit port, a wick is inserted in the neck of the exit needle and lies within the connecting tubing.

The relative flow rates of sheath and sample fluids are determined by differential pressures established by the relative heights of the respective supply reservoirs. Gravity feed was used to establish the flow rates, and a sheath hydraulic head of approximately 70 cm above the exit port produced a sheath flow rate of 1.3 ml/minute. The head of the sample reservoir was approximately 15 cm above the exit port, and it produced a sample flow rate of 0.1 ml per minute.

Light Source

Both coherent (laser) and incoherent (arc or incandescent) light sources are currently used in flow cytometers. The most obvious differences between these light sources are their spectral output and the spatial distribution of the radiation. Each is advantageous for specific flow cytometric applications.

Lasers emit monochromatic light of the same wavelength and phase in a highly collimated beam with a typical diameter less than 2 mm. Thus simple optical arrangements can be used to collect the light and to shape the beam. The principal advantage of lasers is their high energy output ranging from 2 milliwatts to several kilowatts.

In contrast to lasers, incandescent filaments and mercury arc lamps

spontaneously emit atoms at random times. Consequently many continuous, broad spectral bands with several regions of high intensities exist. With the proper choice of filters, light with a range of wavelengths can be selected. Moreover, mercury arc lamps are common, relatively inexpensive source of fluorescence excitation. The major disadvantage of mercury arc lamps is the relatively low luminous intensity obtained when focused to cell-like dimensions. For an in-depth comparison between laser and mercury arc lamp as sources of illumination for flow cytometers, the reader is referred to the article by Peters (46).

In this research, the light source was a Spectra-Physics (Spectra-Physics, Inc., Mountain View, CA) Model 146 helium-neon gas laser with a specified power output of 4 milliwatts at 632.8 nm and a beam diameter at the $1/e^2$ points of 0.922 mm. In the TEM_{00} mode (transverse electric and magnetic modes of oscillations in which there are no transverse nodal lines) the intensity profile across the laser beam is in the form of a bell-shaped or Gaussian distribution which may be expressed by the equation (47):

$$I(R) = I_0 \exp[-2R^2/W^2] \qquad (1)$$

where I_0 is the peak intensity at the center of distribution, R is the radius at which I(R) is calculated and W is the beam radius at the $1/e^2$ point ($0.136I_0$).

Input Beam Optics

In most laser-based flow systems, the 1- to 2-mm diameter light beam emitted by the laser is focused to a small spot, usually slightly larger

than the cell stream. Focusing is usually accomplished by using spherical or cylindrical lenses or a combination of both. Where focusing along one axis is needed, cylindrical lenses are used. Crossing two cylindrical lenses with axes at 90° allows independent focusing in the horizontal and vertical planes. Thus focusing to a spot size with specific major and minor axes can be accomplished with relative ease. In contrast, spherical lenses collimate light to a point source only.

The red light emitted by the helium-neon laser was centered into a 10x microscope objective (N.A. = 0.25) which focused the beam to a point source through a 25 micrometer pinhole which was mounted in a spring loaded, two-way adjustable diameter holder. Both the microscope objective and the pinhole were mounted on the same steel mount with the objective in a fixed position and the pinhole on a stage movable in the horizontal position along the axis of the beam. Thus, fine adjustments could be made via the adjusting screw. The beam coming out of the pinhole was focused onto an achromatic spherical lens (diameter 5.2 cm) approximately 30 cm away from the pinhole. The focal point on the cell stream was found to be approximately 55 cm away from the spherical lens as shown in Figure 3.

The diffraction limited spot diameter can be obtained mathematically by the Airy disc method in which about 80% of the beam energy will be contained in a diameter (47):

$$d_{TEM_{00}} = 2.44f\ \lambda/D \qquad (2)$$

where λ equals the wavelength of light, D equals the diameter of the beam (across the spherical lens), and f equals the focal length of the lens.

With D measuring 5 cm, the beam diameter is calculated to be approximately 17 micrometers, which is smaller than the cell stream (approximately 20 micrometers). To make certain that the beam spot covers the entire flow stream, the beam was defocused slightly by moving the chamber with its detector in the horizontal plane toward the laser.

Photomultiplier Tube and Associated Electronics

In selecting a photomultiplier tube for a particular application, there are a few noteworthy considerations. For example, in low light level applications such as in fluorescence observations, the most important consideration is the effective dark current, which in a photomultiplier tube, is determined by the type and area of the photocathode. When the photomultiplier is operated in complete darkness, electrons are still emitted due to thermionic emission (a function of temperature) which is responsible for the largest component of the dark current. The resulting dark current is amplified by the multiplier system, and therefore sets a limit to the lowest intensity of light that can be detected directly. For applications requiring the maximum signal-to-noise ratio, the dark current can be reduced by cooling the tube or reducing the effective photocathode area by the use of a magnetic lens (48).

Another consideration is the quantum efficiency (Q.E.) defined as the number of photoelectrons emitted from the photocathode per incident photon. The quantum efficiency given in percent at any wavelength can be calculated from the following equation (49):

$$Q.E. = 123.95\ E(\lambda)/\lambda \qquad (3)$$

where $E(\lambda)$ is the photocathode radiant sensitivity expressed in milliamperes per watt and λ is the wavelength in nanometers. Note: $E(\lambda)$ is obtained from the spectral response curve for a particular tube at a specific wavelength. Most Q.E.'s are less than 30% due to imperfect collection and transfer efficiency.

The overall gain (G_1) at a specified voltage (V_1), taking into account losses due to imperfect collection and transfer efficiency, is determined by dividing the anode luminous sensitivity by the cathode luminous sensitivity. Since the photomultiplier tube functions as a photoelectron (current) amplifier with the anode current being a linear function of the input light energy in lumens or watts, it is very sensitive to variations in the applied voltage to the dynode chain. To determine the current gain (G) at some other voltage (V), the following relationship can be used (49):

$$\log_{10} \frac{V}{V_1} = \frac{1}{0.7n} \left(\log_{10} \frac{G}{G_1}\right) \qquad (4)$$

where n is the number of stages of amplification (dynodes).

In this study, the pulses generated by the passing cells were collected by an E.M.I. 9502B (E.M.I. Gencom Inc., Plainview, NY) photomultiplier tube which has a cesium-antimony cathode. The 9502B is a head-on, 50 mm tube with a 10 mm diameter cathode. It is a high gain 13-stage "venetian blind" type tube (designed for low light level applications) with an S-11 spectral response curve shown in the Appendix. The useful range is 300 to 670 nm with a typical Q.E. of 19% at 390 nm. At 632.8 nm (the wavelength of the helium-neon laser), the photocathode

radiant sensitivity is about 3 milliamperes/watt (typical 58 milliamperes/watt at 390 nm) which makes the Q.E., as found from Equation 3, less than 1% (0.59%). Despite the low Q.E., signals for the smallest test particle were well above the noise level (10 millivolts peak-to-peak) with R_f set at 100 kilohms and the photomultiplier tube voltage operated at -860 volts.

Power Supply and Associated Circuitry

To operate a photomultiplier tube, it is necessary to provide interstage voltages to the tube electrodes. This voltage may be supplied by individual sources or by a resistive voltage divider network placed across the high voltage power supply. The value of the resistors is limited at low values by heat dissipation in the divider and the current capacity of the power supply. Generally, resistor values between 20 kilohms and 5 megohms are practical.

Interstage voltages were provided by a nonlinear dynode chain which is particularly suited for pulse counting (48). The divider chain shown in Figure 6 provided sufficient current by using decoupling capacitors in the latter stages to maintain the interstage voltages during the pulse. To maintain the specified cathode to first dynode (K-D1) voltage of 150 volts, a 150 volt Zener diode was employed as the stabilizer which also provided a better signal-to-noise ratio. All of the components for the divider network were mounted at the base of the teflon socket. The chain was operated with the cathode at a negative potential. Consequently, power supply ripple was not injected into the anode circuit.

Enveloping the photomultiplier tube was a shield made of mu-metal

which was maintained at cathode potential and therefore served as an electrostatic as well as a magnetic shield.

The power supply was a HP-6516A (Hewlett-Packard, Palo Alto, CA) which provided a constant, highly stable d.c. voltage. It is well-regulated with low ripple (5 millivolts peak-to-peak). The voltage is also continuously adjustable (0 volt to 3 kilovolts).

Anode Circuit

The output of a photomultiplier is electric charge, and in most applications, this charge is allowed to flow through the load resistor (R_L) while the voltage across it is measured. In this case, the anode was capacitatively coupled to a current-to-voltage transducer using a general purpose operational amplifier (741-type), with the output voltages a direct function of the input currents. Variable gains were provided by feedback resistors of 10 kilohms, 24 kilohms, 56 kilohms, 100 kilohms and 1 megohm. The output from the operational amplifier was coupled to a passive low-pass filter with a cutoff frequency of 15.9 kilohertz to the input of the Tektronix 5103N (Tektronix Inc., Beaverton, OR) oscilloscope which has a bandpass filter that was set from DC to 10 kilohertz. The circuit diagram of the photomultiplier divider network and its anode circuitry appears in Figure 6.

The photomultiplier linearity-gain curve shown in Figure 7 was obtained with the amplifier removed and a 100 kilohm resistor connected across the anode and ground. Neutral density filters (Melles Griot,

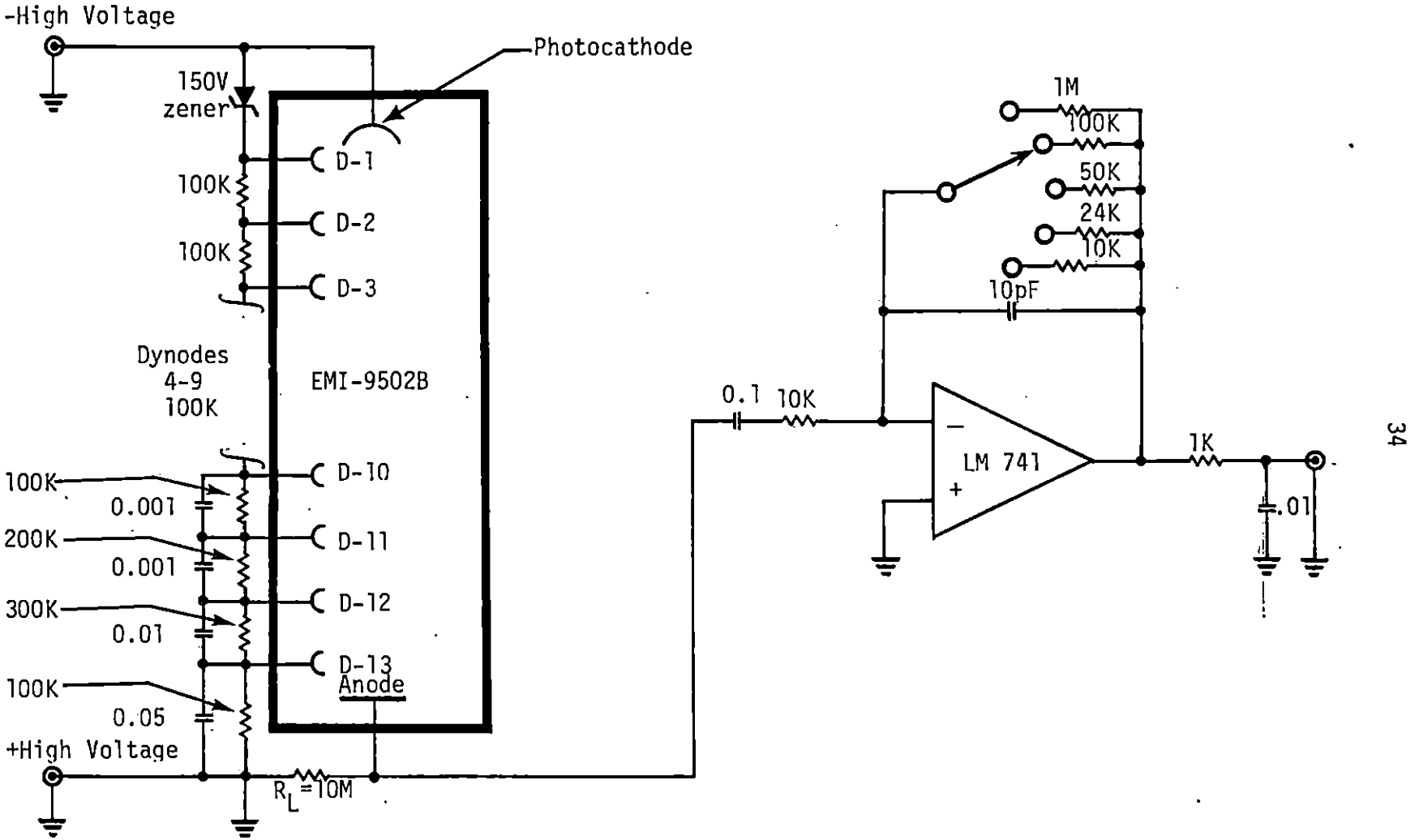

Figure 6. Photomultiplier divider chain and anode circuit.
Resistor values are in Ω and capacitor values are in μF, unless otherwise specified.

Irvine, CA) and a manual chopper were used to respectively attenuate and pulse the focused beam.

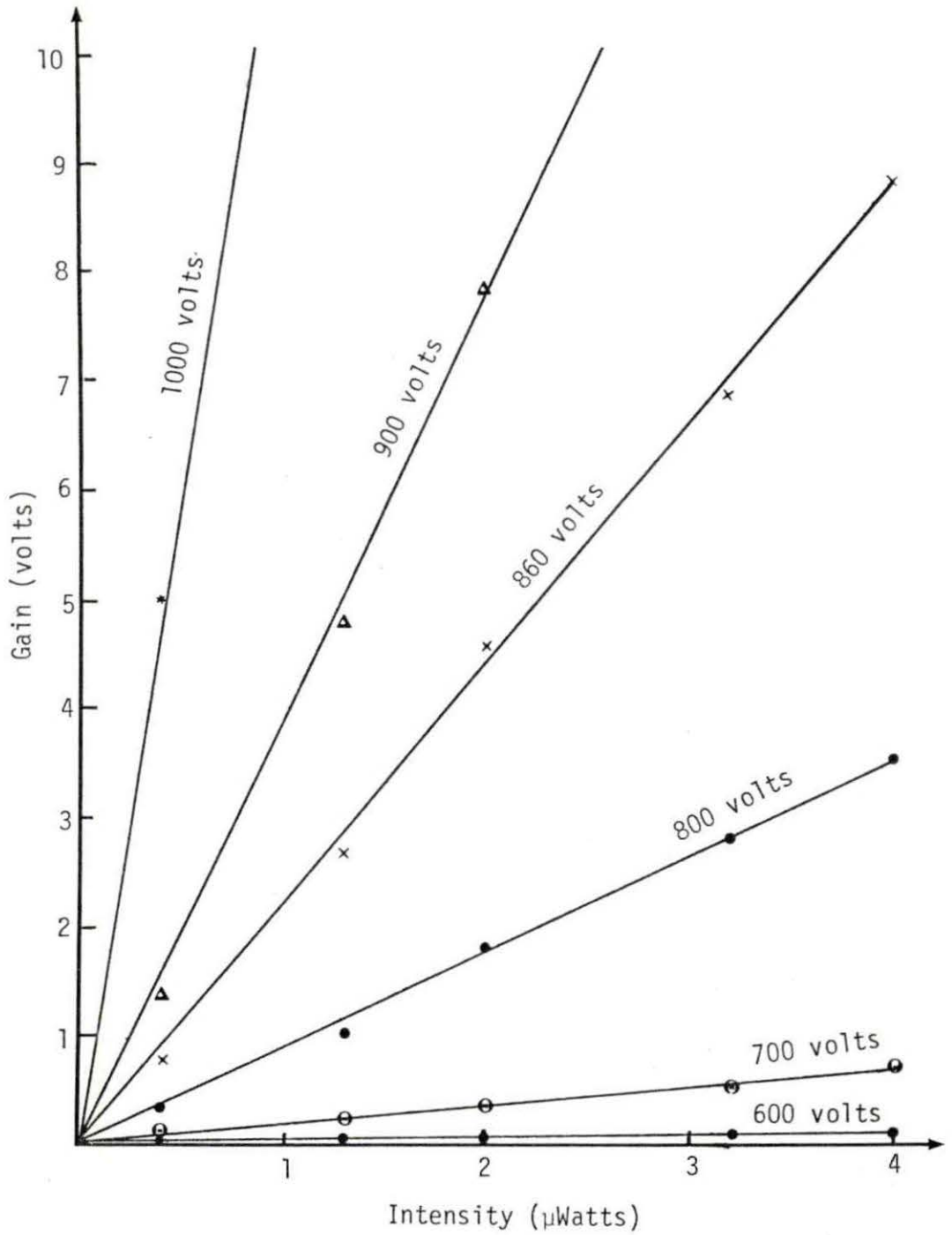

Figure 7. Gain-linearity of PMT with amplifier removed and $R_L \simeq 100k\Omega$. Varying laser intensity was obtained by using Melles Griot neutral density filters and a manual chopper.

EXPERIMENTAL MATERIALS AND METHODS

Whole blood samples collected from dogs and a calf by venipuncture using ethylenediaminetetraacetic acid (EDTA) as an anticoagulant were selected to evaluate the flow chamber described in the previous section. The blood samples were obtained from the Veterinary Diagnostic Laboratory, Iowa State University, Ames, IA after routine differential leukocyte counts and other hematologic determinations such as leukocyte count and hemoglobin concentration had been performed. The records of the laboratory's manually determined differential counts were made available for comparison to the light scatter waveforms obtained from the flow system previously described. Bull sperm cells, collected by electroejaculation, were obtained from the Reproductive Laboratory, Iowa State University, Ames, IA and were also used to evaluate the sensitivity of the system.

Unlike erythrocytes, leukocytes represent a multiclass population, the morphology and ecology of which may give indications of a patient's general state of health or clues to the diagnosis of disease. In normal peripheral blood, there are five different types of mature leukocytes, namely neutrophils, lymphocytes, monocytes, eosinophils and basophils. Each type is found in different concentrations and performs different functions. Table 1 (50) shows the distribution and size of these cells. Even though the leukocyte distributions are different for various species, the size distributions are the same.

The spermatozoon (sperm cell) is a highly specialized cell which has evolved to perform the sole function of fertilizing oocytes. It can be described as having two parts, namely head and tail. The head, which is

Table 1. Differential distribution of dog and cat leukocytes and their respective size. Values in the extreme right column were obtained by measuring the cell diameter from a wet-mount.

	Percentage of each leukocyte			
Cell type	Dog	Calf	Cell size diameter (micrometer) on smear	Measured diameter on wet-mount
Neutrophil	65-70	25-30	10-12	10
Lymphocyte	20-25	60-65	8-15	6
Monocyte	5	5	16-19	13
Eosinophil	2-5	2-5	12-15	-
Basophil	less than 1	less than 1	11-14	-

responsible for penetrating the oocyte to deliver its genetic payload, is 9 micrometers long, 4 micrometers wide and 1 micrometer thick. The tail contains the metabolic machinery to produce energy and to provide the propelling mechanism for motility, and is 57 micrometers long (51).

Prior to each test run, all sheath and diluent fluids were filtered with millipore filters (pore diameter 0.22 micrometer). This helps eliminate extraneous particulate material which would otherwise contribute to the overall noise of the system. Isoton (Coulter Diagnostics, Hialeah, FL), buffered saline with antibacterial and antifungal agents, was used for both the sheath and diluent fluid for the calibration particles, erythrocytes and sperm analysis. However, buffered hypotonic saline (0.40%) was used as the diluent for the leukocyte analysis as suggested by Adams and Kamentsky (52) who were able to cytofluorographically recognize six classes of leukocytes after a brief incubation period in such a fluid.

Alignment of the chamber with the focused beam was performed with the aid of a dissecting microscope positioned in front of the chamber and at approximately 45° to the beam. Both alignment and calibration were performed with a dilute suspension of monodispersed 3.49 micrometer diameter polystyrene particles suspended in filtered Isoton, and introduced in the sample port. Prior to the introduction of the sample, the sheath fluid was allowed to flow for approximately 15 minutes to eliminate air bubbles in the chamber. The sample was then introduced and observed in the transition region found between the sample-sheath assembly and the exit port. During this time the power supply to the photomultiplier tube was turned off to

avoid exposure to the incident beam which would otherwise manifest itself as excessive dark current and cause saturation of the photomultiplier tube. Extreme care was taken to ensure that the beam intersected the central part of the cylindrical flow stream. Once the optical system was aligned, the amplifier and the power supply to the photomultiplier tube were turned on, and the waveforms were observed and photographed from the oscilloscope.

Two sizes of spherical monodispersed latex particles were analyzed. The larger 6 to 14 micrometer diameter particles (Dow Chemical Co., Indianapolis, IN) are styrene divinylbenzene copolymer latexes, whereas the smaller 3.49 micrometer diameter particles (Dow Chemical Co., Indianapolis, IN) are polystyrene latexes. Both sizes were diluted in Isoton. This procedure appeared to provide better monodispersion of the particles than those ultrasonically agitated or treated with a wetting agent such as 95% ethanol.

Since this research dealt with the detection of light scatter from unstained cells, the concentration of cells per unit volume was not ascertained. However, cell suspensions were always checked with a light microscope to verify that cells were separated from each other. At the same time, the cell diameters were measured with an ocular micrometer.

The EDTA anticoagulated blood was allowed to stand in a test tube tilted at a 45° angle for approximately one hour. This allowed the cells to settle into their respective layers: plasma, buffy coat, and red cell layers. Centrifugation to obtain a rich buffy layer caused the white cells to adhere to each other, and also caused physical damage to the cells. Consequently, it was not used. After the buffy coat was visible,

the plasma layer was removed and discarded. The buffy coat was carefully removed with a minimum of red cells and placed in a test tube with about 10 ml of hypotonic saline. Six drops of Zap-oglobin II (Coulter Diagnostics, Hialeah, FL) were added to the test tube, stoppered and mixed. Zap-oglobin II stromatolyses nonnucleated erythrocytes and "reduces cellular debris to an acceptable level" (53). The sample was then transferred to a 50 ml volumetric flask for further dilution and mixing. The final dilution was made such that 5 to 10 leukocytes per high power field could be seen under the microscope. Vigorous shaking was avoided to prevent formation of air bubbles and possible damage to the cells. Once diluted, the specimens were analyzed within half an hour of treatment with Zap-oglobin II, since it also attacks leukocytes.

Since the ratio of red blood cells to leukocytes is about 600 to 1 for dogs and 800 to 1 for calves, no concentration of red blood cells was necessary. The red cell aliquot was taken from the red cell layer and diluted in Isoton.

To avoid carry-over between samples, each successive sample was allowed to flow for about 20 minutes before any data was collected.

To further check the sensitivity of the instrument, bull sperm cells diluted in Isoton were also analyzed. Difficulty was encountered in getting a satisfactory monodispersion of the sperm cells probably due to the seminal fluid and to cold shock after collection. Temperatures lower than body temperature (37° C) appear to influence the agglutination of the sperm cells.

Prior to and at the end of a series of test runs, the 3.49 micrometer

calibration particles were run and the results were recorded. No detectable change in output was observed between calibration particles run either at the beginning or at the end of each test run. Day to day variance was also minimal.

RESULTS

Signal waveforms representing light scatter signatures of latex spheres, bull sperm cells, red blood cells and leukocytes appear in Figures 8 through 17. Scale factors are indicated on each figure.

After initial alignment and calibration, the system remained unchanged. The high voltage to the photomultiplier tube was set at -860 volts, R_f set at 100 kilohms and the relative heights of the sample and sheath reservoirs were held constant for each test. The triggering level on the oscilloscope was also held constant for all calibration and test sample runs.

Each waveform can be described according to its height, width and shape. The height represents light scattering due to the size of the particle, the width represents the cell transit time across the beam, and the shape represents the trajectory path of the cell across the beam. Cells in the center of the cylindrical stream have shorter transit times than those at the periphery of the stream and give the most symmetrical pulses as seen in the work of Von Behrens and Edmondson (27). Lighter areas indicate the frequent occurrence of particles of the same size, and the darker area indicate particles of different sizes.

Figure 8 represents light scattered by uniform 3.49 micrometer latex spheres. Amplitudes appear to vary from 225 to 275 millivolts.

Figure 9 supposedly represents 6 to 14 micrometer latex spheres but the smaller 225 millivolt waveforms indicate the presence of particles smaller than 6 micrometers. Microscopic examination of an aliquot of the stock solution indicated the presence of 3.49 micrometer latex spheres.

Figure 8. Signal waveforms of 3.49 micrometer latex spheres.
Exposure time = 10 seconds.
Photomultiplier tube voltage = -860 volts.
Operational amplifier R_f = 100 kilohms.

Figure 9. Signal waveforms of 6 to 14 micrometer latex spheres.
Exposure time = 10 seconds.
Photomultiplier tube voltage = -860 volts.
Operational amplifier R_f = 100 kilohms.

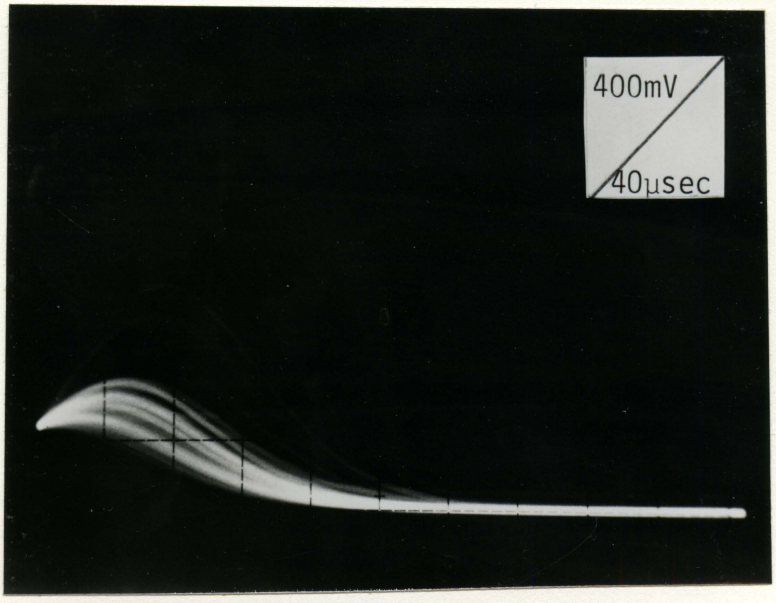
400mV
40μsec

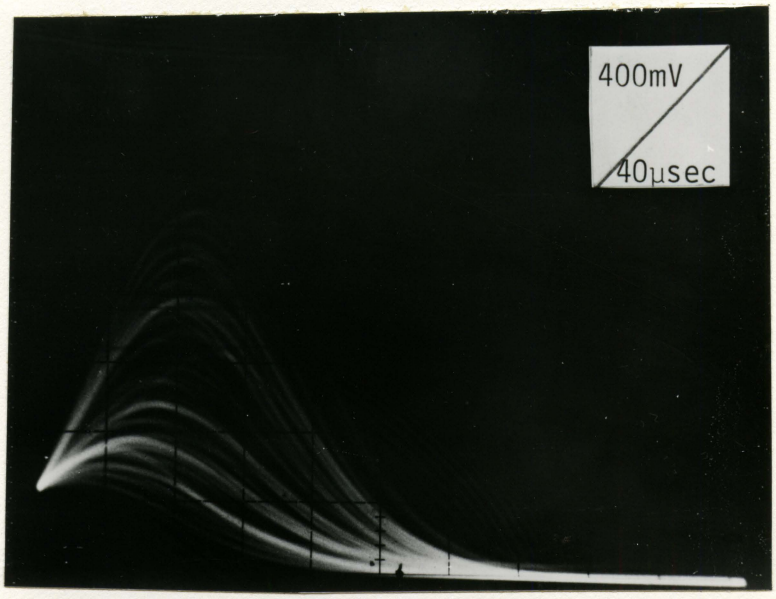
400mV
40μsec

Figure 10. Signal waveforms of a mixture of 3.49 micrometer and 6 to 14 micrometer latex spheres.
Exposure time = 10 seconds.
Photomultiplier tube voltage = -860 volts.
Operational amplifier R_f = 100 kilohms.

Figure 11. Signal waveforms of bull sperm cells.
Exposure time = 10 seconds.
Photomultiplier tube voltage = -860 volts.
Operational amplifier R_f = 100 kilohms.

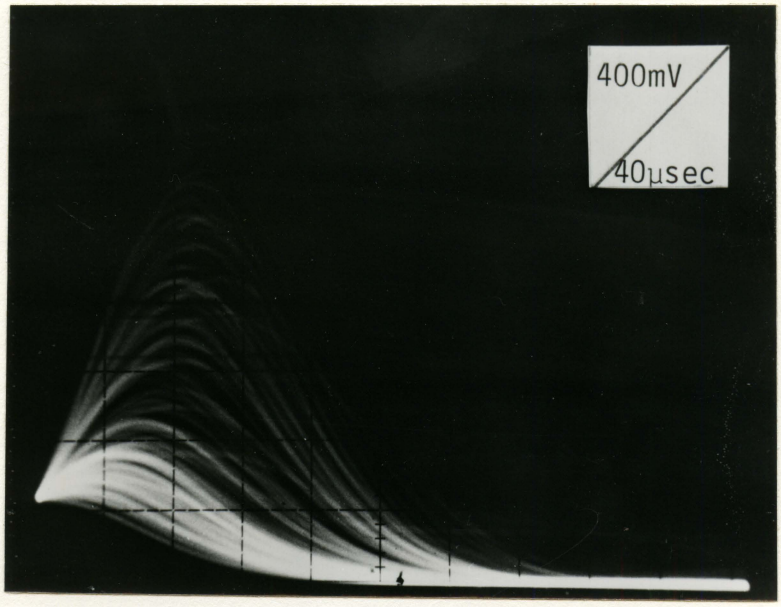
400mV
40μsec

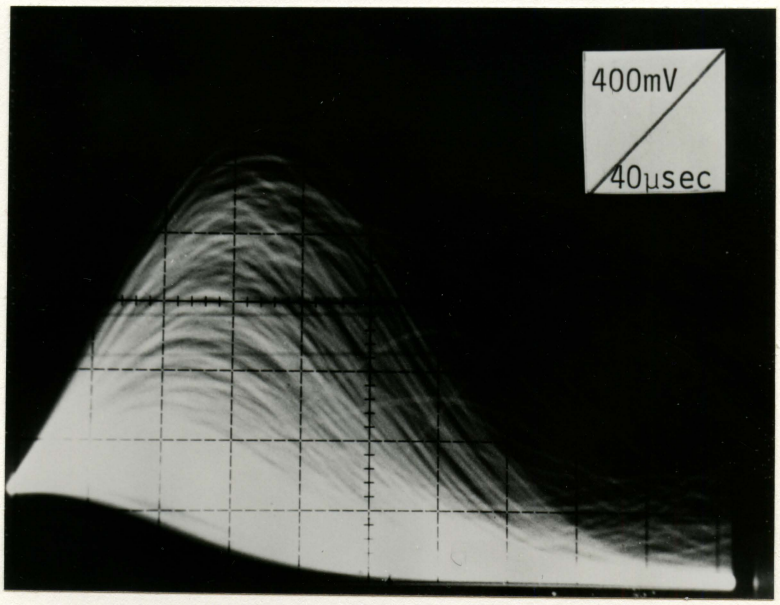
400mV
40μsec

Figure 12. Signal waveforms of calf erythrocytes
(measured diameter = 5 micrometers).
Exposure time = 10 seconds.
Photomultiplier tube voltage = -860 volts.
Operational amplifier R_f = 100 kilohms.

Figure 13. Signal waveforms of dog erythrocytes
(measured diameter = 7.5 micrometers).
Exposure time = 10 seconds.
Photomultiplier tube voltage = -860 volts.
Operational amplifier R_f = 100 kilohms.

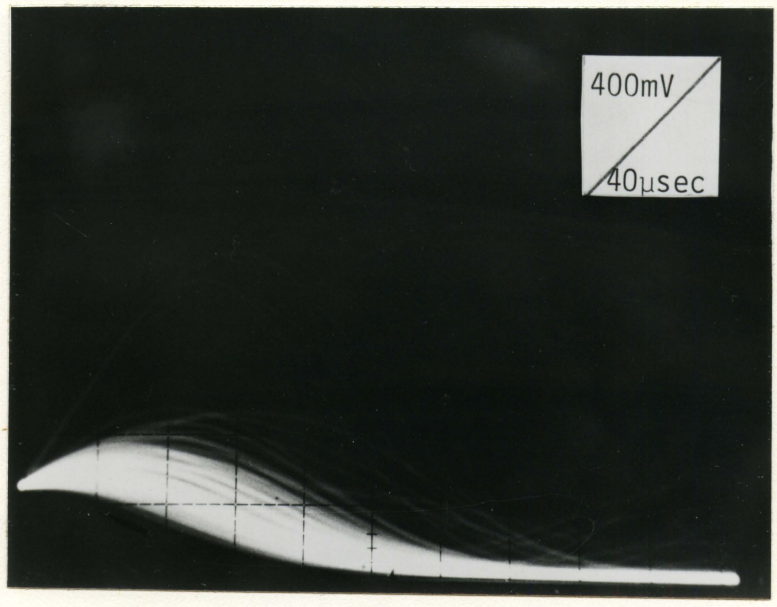
400mV
40μsec

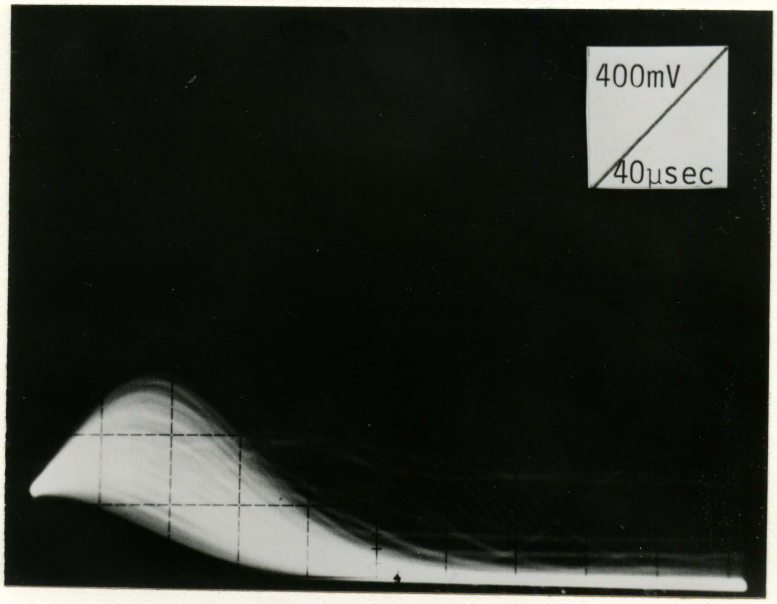
400mV
40μsec

Figure 14. Signal waveforms of dog leukocytes.
Differential count from wedge smear: 45% neutrophils, 45% lymphocytes, 5% monocytes, 2% basophils and 3% eosinophils.
Exposure time = 10 seconds.
Photomultiplier tube voltage = -860 volts.
Operational amplifier R_f = 100 kilohms.

Figure 15. Signal waveforms of dog leukocytes.
Differential count: 92% neutrophils and 8% lymphocytes.
Exposure time = 15 seconds.
Photomultiplier tube voltage = -860 volts.
Operational amplifier R_f = 100 kilohms.

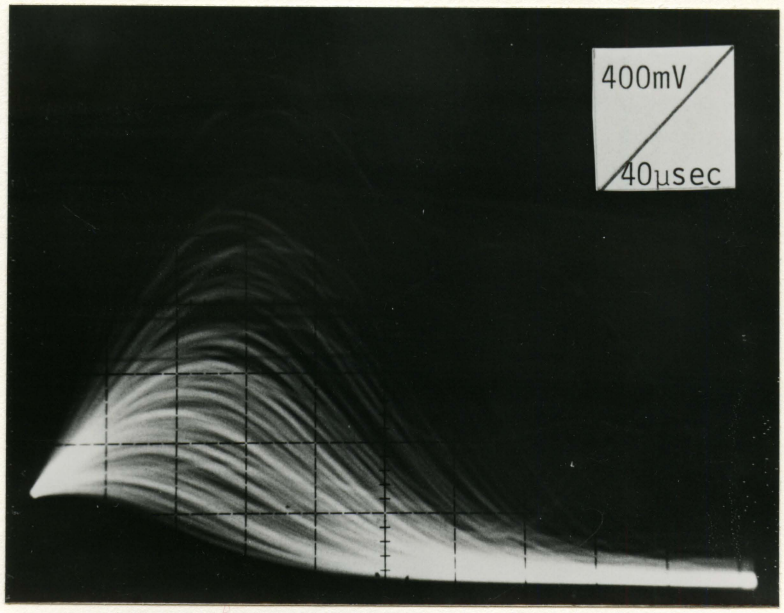
400mV
40μsec

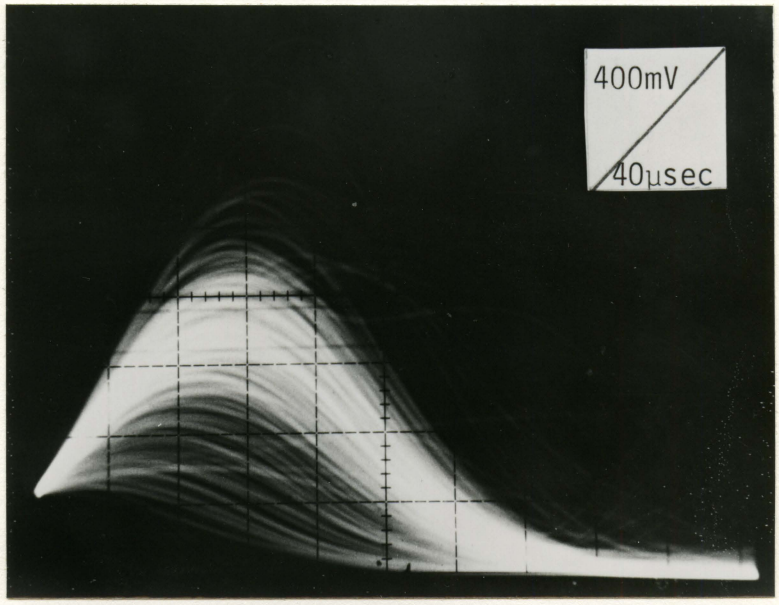
400mV
40μsec

Figure 16. Signal waveforms of calf leukocytes.
Differential count: 21% neutrophils, 8% bands, 71% lymphs.
Exposure time = 10 seconds.
Photomultiplier tube voltage = -860 volts.
Operational amplifier R_f = 100 kilohms.

Figure 17. Signal pulses of calf leukocytes along with other particulate materials.
Exposure time = 200 milliseconds.
Photomultiplier tube voltage = -860 volts.
Operational amplifier R_f = 100 kilohms.

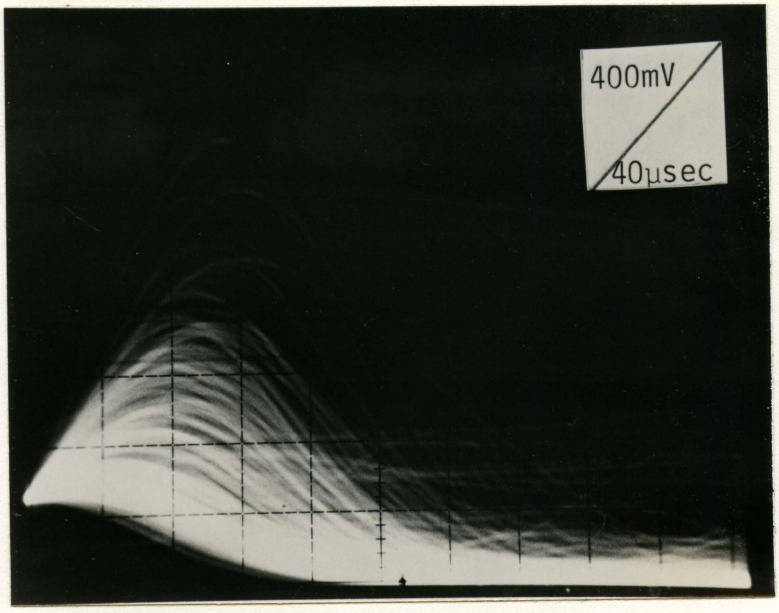
400mV
40μsec

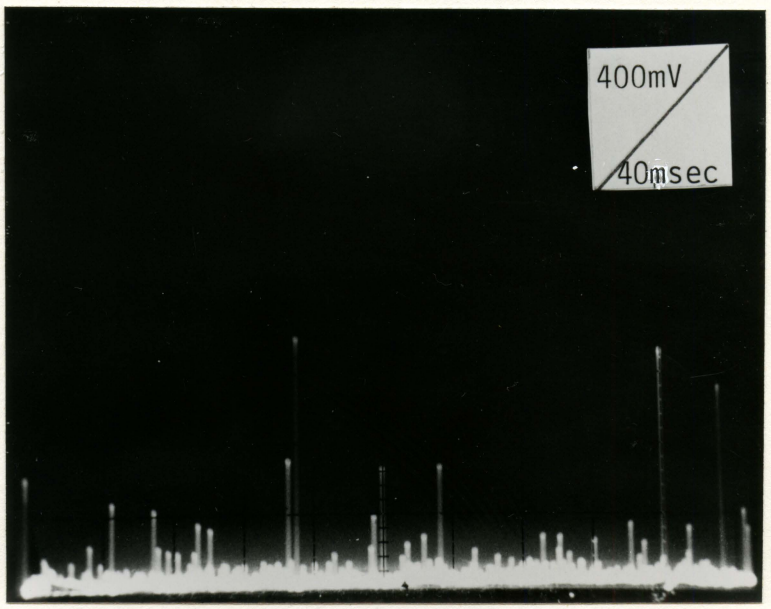
400mV
40msec

Figure 10 shows the combined waveforms seen in Figures 8 and 9. Equal volumes of dilute monodispersed 3.49 micrometer and 6 to 14 micrometer latex spheres, used previously to obtain the waveforms of Figures 8 and 9 respectively, were mixed and sampled. Note the smaller lighter waveforms indicating the presence of more 3.49 micrometer spheres than in Figure 8.

The waveforms of the bull sperm cells seen in Figure 11 indicate that only the heads scattered enough light to be detected by the existing system. The heads, which are approximately the size of red blood cells, produce signal waveforms which are similar to those shown in Figures 12 and 13, except for the larger waveforms which are probably due to doublets (two cells stuck together), triplets (three cells stuck together) and white cells going through the laser beam.

Figure 12 represents the waveforms of calf erythrocytes with an average measured diameter of 5 micrometers.

Figure 13 represents the waveforms of dog erythrocytes with an average measured diameter of 7.5 micrometers.

Figures 14 through 18 represent specimens with different leukocyte distributions. In each case, a blood smear was prepared and stained with Wright's blood stain, a two component polychrome dye. The slides were examined at 1000x magnification using oil immersion microscopy, and differential counts based on identification of only the first 100 cells were done.

Figure 14 represents the light scatter waveforms from dog leukocytes which had the following differential count: 45% neutrophils, 45% lympho-

cytes, 5% monocytes, 2% basophils and 3% eosinophils. Differences in waveforms are not obvious until they are compared to those seen in Figures 15 and 16.

Figure 15 represents the waveforms obtained from a different dog whose leukocytes were predominantly neutrophils (differential count: 92% neutrophils, 8% lymphocytes).

Figure 16 represents the waveforms obtained from calf leukocytes which had an abundance of small lymphocytes measuring approximately 6 micrometers. The differential count was 21% neutrophils, 8% bands (jeuveniles) and 71% lymphocytes.

Finally, Figure 17 shows the number of leukocytes present along with other cells and debris. The smaller pulses (less than 150 millivolts) are probably due to red blood cell fragments left after saponification with Zap-oglobin II, and also to platelets which are found in high concentration in the buffy coat along with the white cells. The intermediate (200-400 millivolts) pulses are probably due to the lymphocytes and the larger (600-800 millivolts) pulses to the neutrophils.

DISCUSSION

Calibration of the system was based on the waveforms seen in Figure 8. These waveforms were obtained from the light scatter signals of uniform 3.49 micrometer latex spheres. Ideally one would expect to see a single waveform, rather than several waveforms with amplitudes varying from 225 to 375 millivolts and transit times from 80 to 90 microseconds. These variations are probably due to fluctuations in the flow stream and to variations in the flow path of the cells within the illuminated portion of the flow stream. As discussed earlier, those particles in the center of the flow stream have the shortest transit times and consequently have narrower pulses than those at the periphery. Figure 8 also includes waveforms that appear to be approximately 500 millivolts, probably due to doublets crossing the beam.

Using the data obtained for the 3.49 micrometer particles, and assuming that the pulse heights are linearly related to the size of the particles, the following equation can be used to compute the size of the tested particles:

$$\text{Particle size (micrometers)} = \frac{3.49 \text{ (micrometers)}}{300 \text{ (millivolts)}} \times \text{Pulse height (millivolts)} \qquad (5)$$

where 3.49 micrometers is the size of the calibration particles, 300 millivolts is the mean amplitude of waveforms obtained from those particles, and Pulse height is the mean amplitude of the waveforms of particles of unknown size.

The linearity of the system was checked with 6 to 14 micrometer

latex spheres. Figure 9 represents the waveforms obtained from 6 to 14 micrometer spheres. The amplitudes of the waveforms appear to vary from 225 to 1200 millivolts. Using equation 5, the computed size range of the particles are 2.60 to 13.96 micrometers. The upper range (13.96 micrometers) is in good agreement with the specified 14 micrometer value. The computed lower range (2.60 micrometers) obviously represent particles smaller than 6 micrometers. Microscopic examination and measurement of an aliquot of the diluted 6 to 14 micrometer sample and of the stock solution showed the presence of 3.49 micrometer particles.

Figure 10 represents waveforms obtained from mixing equal parts of diluted 3.49 micrometer and 6 to 14 micrometer suspensions which were used to obtain the waveforms seen in Figures 8 and 9. Figure 10 is clearly an effective composite of the waveforms for the 3.49 micrometer particles. This further supports the suggestions that 3.49 micrometer particles are contaminants in the 6 to 14 micrometer stock solution.

Figure 11 represents waveforms resultant from the use of sperm cells as test particles. There are numerous waveforms in Figure 11 with amplitudes varying from 225 to 500 millivolts. Waveforms with a mean amplitude of 363 millivolts represent computed particle size of 4.2 micrometers which is in the size range of the head of the bull sperm cells. The larger waveforms (450 to 1200 millivolts) are probably due to doublets and triplets, and to white cells which are normally found in semen samples. Light scattered by the long (57 micrometer, McDonald 1980) slender tails of the sperm cells were not detected; otherwise, one would expect long transit time pulses generated by such structures.

Figures 12 and 13 represent waveforms obtained from red blood cells of a calf and a dog, respectively. In the first case the red blood cells were from a two-week old calf. Microscopic examination of these cells showed the presence of microcytes (cell diameter less than 6 micrometers) with slight anisocytosis. The waveforms in Figure 12 appear to vary from about 250 to 375 millivolts which yields a predicted size of 2.9 to 4.4 micrometers. The average measured size of the calf red blood cells was 5 micrometers. The waveforms of the dog red blood cells appear to have amplitudes varying from 250 to 500 millivolts as seen in Figure 13. Again using equation 5, the predicted range of values is 2.9 to 5.8 micrometers (mean 4.4 micrometers) compared to the average measured 7.5 micrometer diameter. The differences in the predicted and measured values of the red cells are probably due to the shape, effects of orientation of the particles in the cell stream and also to the flight path of the particle across the stream. If, however, the data obtained from calf blood are used as a proportional factor (5 micrometers/300 millivolts), the average predicted value for dog erythrocyte would be 6.1 micrometers.

Figure 14 represents canine leukocytes of mixed distribution which makes it difficult to associate specific waveforms with specific cell types. However, based on the differential count, one can suggest that waveforms with peak amplitudes from 250 to 800 millivolts represent neutrophils and lymphocytes. The larger waveforms (900 to 1050 millivolts) probably represent monocytes. The average predicted value of monocyte is 10.9 micrometers compared to the measured 13 micrometer diameter.

The waveforms which probably represent neutrophils in Figure 15

appear to have peak amplitudes ranging from 575 to 850 millivolts with a predicted size of 6.7 to 9.9 micromters. The mean measured value is seen in Table 2.

The amplitudes of the suspected lymphocyte waveforms seen in Figure 16 are identical to the calf red cell waveforms seen in Figure 12. The peak amplitudes range from 250 to 375 millivolts, which yields a predicted range of 2.9 to 4.4. micrometers (mean 3.6 micrometers) as opposed to the measured 6 micrometer diameter.

Experimental results, along with the predicted and measured cell diameters are summarized in Table 2. The predicted diameter values of the mixed latex spheres are in close agreement with the measured diameter, whereas the correlation for biological cells seem to vary from 12% to 41%. This wide variance is probably due to shape and internal structures of the cells.

Eosinophils and basophils were not identified due to their overlapping size with neutrophils and their low incidence of occurrence in normal circulating blood.

Flow systems designed for rapid individual cell analysis require that cell samples consist of monodispersed cells suspended in a liquid medium Therefore, sample preparation in the disaggregation of cells into single cell entities plays an extremely critical role. Whole blood samples appear to produce cells that are easily separated from each other, unlike bovine cells which have a tendency to clump. Part of this problem may be attributed to improper specimen handling after collection. Instead of exposing the specimen to cold shock which enhances clumping, the specimen

Table 2. Predicted and experimental values of test particles.

Figure #	Peak amplitude (millivolts)		Predicted cell diameter (micrometers)		Measured diameter (micrometers)	Comment
	Range	Mean	Range	Mean	Mean	
9	225-1200	713	2.6-14.0	-	3.49-13	Latex sphere
10	225-1200	713	2.6-14.0	-	3.49-13	Latex sphere
11	225- 500	363	2.6- 5.8	4.2	5(W) x 9(L)	Head of bovine sperm cell
12	250- 375	313	2.9- 4.4	3.7	5	Bovine erythrocyte
13	250- 500	375	2.9- 5.8	4.4	7.5	Canine erythrocyte
14	900-1050	975	10.5-12.2	11.4	13	Monocyte
15	575- 850	713	6.7- 9.9	8.3	10	Neutrophil
16	250- 375	313	2.9- 4.4	3.7	6	Lymphocyte

should be stored as close to body temperature as possible until it is time be used.

Background noise also reduces the overall quality of the instrument. It may manifest itself as microbubbles in the sample and/or diluent fluids. Microbubbles can be prevented by gently, instead of vigorously, mixing the respective fluids.

Particulate matter in the sheath and diluent fluid also reduces overall quality of the system. Filtering with millipore filters removes unwanted debris. However, filtering the diluent does not prevent bacterial growth which also contributes to the overall noise. The use of Isoton seems to solve this problem.

SUMMARY AND CONCLUSIONS

A sheath flow chamber, constructed from Plexiglas and hypodermic needles, was used to confine cells in the center of a coaxial flow stream for exposure to the focused beam of the 632.8 nm wavelength light from a helium-neon laser. Forward light scatter signals were collected by a photomultiplier tube. The signals were amplified, filtered and photographed from an oscilloscope.

Lighter scattering results from latex particles and unstained biological cells indicate a linear correlation between the peak amplitudes of the output waveforms.

RECOMMENDATIONS FOR FURTHER STUDY

Numerous suggestions could be made to improve the existing system. Starting with the optics, cylindrical lenses could be used to focus the laser beam to a narrow ellipse as large as the entire cell stream in the horizontal direction. This would ensure complete illumination of the entire flow stream, thus greatly improving the resolution of the system.

To further improve the signal-to-noise level, the photomultiplier tube should be operated at or near optimal level, that is, the light source should spectrally complement the detector. Substituting a different light source such as a helium-cadmium laser in combination with the existing E.M.I. 9502B photomultiplier tube could greatly improve the signal-to-noise ratio.

Instead of gravity feed for hydrodynamic focusing, constant pressure reservoirs could greatly minimize fluctuations in the sample and sheath flow which were probably partially responsible for the variation of the acquired data (33).

Light scattering signatures at one fixed angle do not yield enough information to accurately identify different cell types. However, if they are augumented with fluorescence and/or absorption, or even angular light scatter, more information could be obtained. This would, of course, complicate the data acquisition process. By interfacing the system to a minicomputer, various algorithms could be selected to accurately identify the cells of interest.

Finally, to improve the light collection efficiency of the system, a spherical mirror could be used to collect back-scatter light, which

together with forward scatter could greatly minimize the effects due to orientation of the particles in the cell stream.

BIBLIOGRAPHY

1. Mullaney, P. F., and P. N. Dean. 1970. The small angle light scattering of biological cells. Theoretical considerations. Biophysics J. 10:764-772.

2. Brunsting, A., and P. F. Mullaney. 1972. Light scattering from coated spheres: a model for biological cells. Applied Optics 11:675.

3. Crosland-Taylor, P. J. 1953. A device for counting small particles suspended in a fluid through a tube. Nature 171:37-38.

4. Jovin, T. M., S. J. Morris, G. Striker, H. A. Schultens, M. Digweed, and D. J. Arndt-Jovin. 1976. Automatic sizing and separation of particles by ratios of light scattering intensities. J. Histochem. Cytochem. 24:269-283.

5. Loken, M. R., and L. A. Herzenberg. 1975. Analysis of cell populations with a fluorescence-activated cell sorter. Ann. N. Y. Acad. Sci. 254:263.

6. Loken, M. R., R. G. Sweet, and L. A. Herzenberg. 1976. Cell Discrimination by multiangle light scattering. J. Histochem. Cytochem. 24(1):284-291.

7. Cram, L. S., and A. Brunsting. 1973. Fluorescence and light scattering measurements on hog cholera-infected PK-15 cells. Exptl. Cell Res. 78:209.

8. Kay, D. B., and L. L. Wheeless. 1976. Laser stroboscopic photography technique for cell orientation studies in flow. J. Histochem. Cytochem. 24:265.

9. Loken, M. R., D. R. Parks, and L. A. Herzenberg. 1977. Identification of cell asymmetry and orientation by light scattering. J. Histochem. Cytochem. 25(7):790-795.

10. Jenkins, F. A., and H. E. White. 1976. Fundamentals of Optics. McGraw-Hill Book Company, New York. 746 pp.

11. Salzman, G. C., J. M. Cromwell, C. A. Goad, K. M. Hansen, R. D. Hiebert, P. M. LaBauve, J. C. Martin, M. L. Ingram, and P. F. Mullaney. 1975. A flow-system multiangle light-scattering instrument for cell characterization. Clin. Chem. 21(9):1297-1304.

12. Kerker, M. 1969. The Scattering of Light and Other Electromagnetic Radiation. Academic Press, New York. 666 pp.

13. Wyatt, P. J. 1968. Differential light scattering: a physical method for identifying bacterial cells. Applied Optics 7(10): 1879-1896.

14. Blum, L. L. 1945. The photoelectric determination of erythrocyte count. Am. J. Clin. Pathol. 15:85-93.

15. Moldavan, A. 1934. Photo-electric technique for the counting of microscopial cells. Science 80:188-189.

16. Gucker F. T., Jr., C. T. O'Konski, H. B. Pickard, and J. N. Pitts, Jr. 1947. A photoelectric counter for colloidal particles. J. Am. Chem. Soc. 69:2422-2431.

17. Lagercrantz, C. 1948. Photo-electric counting of individual microscopic plant and animal cells. Nature 161:25-26.

18. Reynolds, O. 1883. An experimental investigation of the circumstances which determine whether the motion of water shall be direct or sinous, and of the law of resistance in channels. Phil. Trans. 935.

19. Frommer, P. L. 1955. An electronic blood-count meter. Electrical Engineering 74:388-391.

20. Steinkamp, J. A. 1967. An apparatus for the detection of fluorescing cells. M.S. Thesis. Iowa State Univ., Ames, IA.

21. Coulter, W. H. 1956. High speed automatic blood cell counter and cell size analysis. Proc. Natl. Electron. Conf. 12:1034-1042.

22. Kubitschek, H. E. 1958. Electronic counting and sizing of bacteria. Nature 182:234-235.

23. Sipe, C. R., and E. P. Cronkite. 1962. Studies on the application of the Coulter electronic counter in enumeration of platelets. Anal. N. Y. Acad. Sci. 99(1-3):262-269.

24. Segal, S.J., and K. A. Lawrence. 1962. Automatic analysis of particulate matter in human semen. Anal. N. Y. Acad. Sci. 99(1-3): 271-279.

25. Hastings, J. W., B. M. Sweeney, and M. M. Mullin. 1962. Counting and sizing of unicellular marine organisms. Anal. N. Y. Acad. Sci. 99(1-3):280-289.

26. Kachel, V. 1976. Basic principles of electrical sizing of cells and particles and their realization in the new instrument "Metricell". J. Histochem. Cytochem. 24(1):211-230.

27. Von Behrens, W., and S. Edmondson. 1976. Comparison of techniques improving the resolution of standard Coulter cell sizing systems. J. Histochem. Cytochem. 24(1):247-256.

28. Leary, J. F., P. Todd, J. C. S. Wood, and J. H. Jett. 1979. Laser flow cytometric light scatter and fluorescence pulse width and pulse rise-time sizing of mammalian cells. J. Histochem. Cytochem. 27(1):315-320.

29. Kamentsky, L. A., M. R. Melamed, and H. Derman. 1965. Spectrometer: new instrument for ultrarapid cell analysis. Science 150:630-631.

30. Van Dilla, M. A., T. T. Trujillo, P. F. Mullaney, and J. R. Coulter. 1969. Cell Microfluorometry: A method for rapid fluorescence measurement. Science 163:1213-1214.

31. Mullaney, P. F., M. A. Van Dilla, J. R. Coulter, and P. N. Dean. 1969. Cell sizing: a light scattering photometer for rapid volume determination. Rev. Sci. Instr. 40:1029-1032.

32. Mellors, R. C., and R. Silver. 1951. A microfluorometric scanner for the differential detection of cells: Application to exfoliative cytology. Science 114:356-360.

33. Melamed, M. R., P. F. Mullaney, and M. L. Mendelsohn. 1979. Flow Cytometry and Sorting. Wiley and Sons, New York. 716 pp.

34. Holm, D. M., and L. S. Cram. 1973. An improved flow microfluorometer for rapid measurement of cell fluorescence. Exptl. Cell Res. 80:105-110.

35. Mullaney, P.F., and W.T. West. 1973. A dual-parameter flow microfluorometer for rapid cell analysis. J. Phys. 6:1006-1008.

36. Steinkamp, J. A., and A. Romero. 1974. Identification of discrete classes of normal human peripheral lymphocytes by multiparameter flow analysis. Proc. Sci. Exper. Bio. Med. 146:1061-1066.

37. Arndt-Jovin, D. J., and T. M. Jovin. 1974. Computer-controlled multiparameter analysis and sorting of cells and particles. J. Histochem. Cytochem. 22(7):622-625.

38. Mansberg, H. P., A. W. Saunders, and W. Groner. 1974. The Hemalog D white cell differential system. J. Histochem. Cytochem. 22(7): 711-724.

39. Salzman, G. C., J. M. Cromwell, J. C. Martin, T. T. Trijillo, A. Romero, P. F. Mullaney, and P. M. LaBauve. 1975. Cell classification by laser light scattering: identification and separation of unstained leukocytes. Acta Cytologica 19(4):374-377.

40. Eisert, W. G., R. Osterag, and E. G. Niemann. 1975. Simple flow microphotometer for rapid cell population analysis. Rev. Sci. Instr. 46(8):1021-1024.

41. Skogen-Hagenson, M. J., G. C. Salzman, P. F. Mullaney, and W. H. Brockman. 1977. A high efficiency flow cytometer. J. Histochem. Cytochem. 25(7):784-789.

42. Lindmo, T., and H. B. Steen. 1979. Flow cytometry: a high-resolution instrument for everyone. Science 204(27):403-404.

43. Hercher, M., W. Mueller, and H. M. Shapiro. 1979. Detection and discrimination of individual viruses by flow cytometry. J. Histochem. Cytochem. 27(1):350-352.

44. Bonner, W. A., H. R. Hulett, R. G. Sweet, and L. A. Herzenberg. 1972. Fluorescence activated cell sorting. Rev. Sci. Instr. 43:404-409.

45. Kamentsky, L. A. 1979. Future directions for flow cytometry. J. Histochem. Cytochem. 27:1649-1651.

46. Peters, D. C. 1979. A comparison of mercury arc lamp and laser illumination for flow cytometers. J. Histochem. Cytochem. 27(1): 241-245.

47. Goldman, L., and R. J. Rockwell, Jr. 1971. Lasers in Medicine. Gordon and Breach, Science Publishers, Inc., New York. 385 pp.

48. E.M.I. ca. 1965. An introduction to the photomultiplier. E.M.I. Gencom Inc., Plainview, New York.

49. E.M.I. ca. 1977. Photomultiplier tubes. E.M.I. Gencom Inc., Plainview, New York.

50. Schaln, O. W., N. C. Jain, and E. J. Carroll. 1975. Veterinary hematology. Lea and Febiger, Philadelphia. 807 pp.

51. McDonald, L. E. 1980. Veterinary endocrinology and reproduction. Lea and Febiger, Philadelphia. 560 pp.

52. Adams, L. R., and L. A. Kamentsky. 1974. Fluorometric characterization of six classes of human leukocytes. J. Histochem. Cytochem. 18:389-391.

53. Coulter Diagnostics. 1977. Zap-isoton II and Zap-oglobin II. Coulter Diagnostics, Hialeah, Florida.

ACKNOWLEDGEMENTS

The author wishes to acknowledge his sincere appreciation to the many people, including the Faculty and Staff of the Biomedical Engineering Program, for their support and advice throughout this research program.

I am especially grateful to my major professor, Dr. W. H. Brockman for his guidance during this study, and for reviewing and editing this manuscript.

Thanks to Dr. D. L. Carlson for his counselling and guidance, and Dr. L. Y. Quinn for serving on my committee.

I am also thankful to Deb Hoyt for providing the blood samples and Dr. L. Evans for the bovine sperm sample.

Last but not least, special gratitude is extended to my wife, Carla for typing this thesis and for her patience and sacrifices during my graduate studies.

APPENDIX

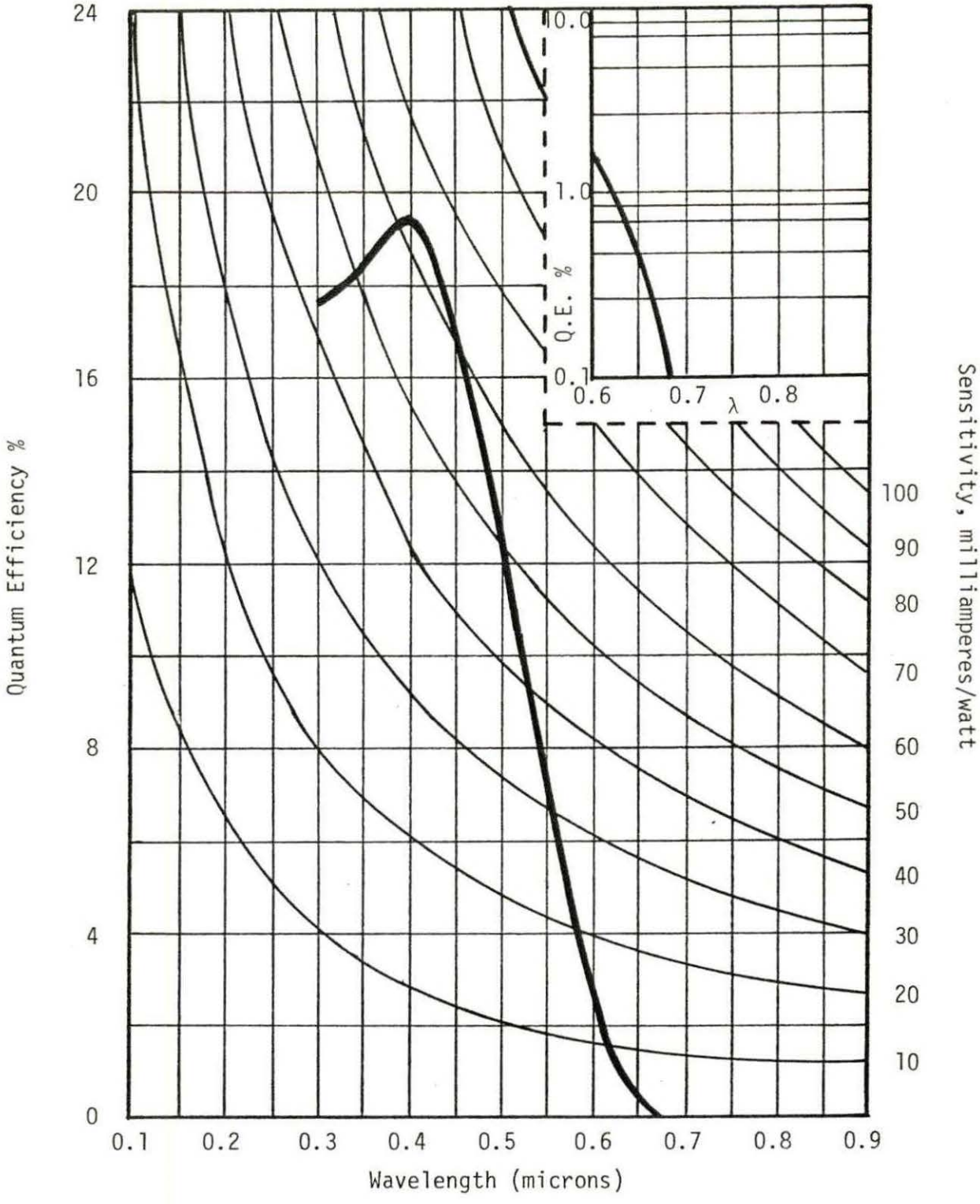

Figure A1. Spectral response of the E.M.I. 9502B photomultiplier tube.